Microgravity Environment of the Material Science Double Rack on Spacelab-1

H. Hamacher*
Deutsche Forschungs- und Versuchsanstalt für Luft- und Raumfahrt
Cologne, Federal Republic of Germany
and
U. Merbold†
European Space Agency, Paris, France

The Material Science Double Rack, a payload element of the STS-9/Spacelab-1 Mission, was equipped with a three-axis acceleration sensor for measuring the residual acceleration (μg-field). Peak values of the μg-field within intervals of $\Delta t = 1$ s were detected between 10^{-5} and $10^{-2}\ g_o$. In the first part of this paper, a review of main types of μg-disturbances is given, followed by a description of the accelerometer system and those STS-9 features of interest to this discussion. Then, SL-1 μ data are analyzed with respect to mission events by correlation with the as-flown timeline. The origins of disturbances are divided into orbit-, vehicle-, and experiment-induced perturbations. It has been found that the μg-environment is dictated mainly by payload-induced perturbations with the exception of one Orbit Trim Burn. To reduce the μg-levels, the design of some experiment facilities has to be improved by minimizing the number of moving parts, decoupling disturbing units from experiment facilities, taking damping measures, etc. In addition, strongly disturbing experiments and very sensitive investigations should be performed in separate mission phases.

Nomenclature

$\hat{a}$	= peak value detected during $\Delta t = 1$ s
$\bar{a}_c$	= acceleration due to Orbiter rotation
$\bar{a}_d$	= acceleration due to atmospheric drag
$\bar{a}_{\min}$	= lowest detectable value of $\hat{a}$
$\bar{a}_t$	= tidal acceleration
$a_{t,z}$	= component of $\bar{a}_t$ in the direction of $\bar{R}$
d	= defined in Fig. 2
g_o	= 9.81 m s^{-2} gravitational acceleration at the Earth surface
h	= altitude
k	= defined in Eq. (1)
m	= Orbiter mass
r	= position vector from CM to the object
$r_{o,\mathrm{CM}}$	= position vector of CM in the OSCS
R	= position vector from the center of Earth to CM
r_z	= component of r in the direction of R
u,v,w	= coordinate system of the μg-sensor
x_o,y_o,z_o	= Orbital Structural Coordinate System (OSCS)
ω	= angular velocity

Introduction

SPACELAB-1, flown November 28 through December 8, 1983, was the first of a series of Spacelab Missions in which the complex laboratory built by the European Space Agency was used. The flight presented a first opportunity to carry out research in the special environment of orbital flight, using a laboratory specifically designed for scientific experiments. From a total of 70 successfully performed investigations, 39 experiments in the area of materials sciences and fluid physics were carried out, making use of the greatly reduced level of gravitational force aboard an orbiting spacecraft.[1] Most of these experiments were performed in shared facilities that were part of the Material Science Double Rack (MSDR), a payload element consisting of several furnaces, process chambers, and related subsystems. The MSDR was also equipped with a three-axis acceleration sensor for measuring the residual acceleration continuously over the experiment operation time. The results of these measurements are primarily an important basis for the scientific analysis of the experiments performed. The μg-data are, on the other hand, valuable for examining and improving the design and operational concept of a payload.

In this paper, some characteristic features and results of the SL-1 μg-measurements will be presented and discussed. Starting with a brief review of the main potential disturbances, the payload aspects of interest to the analysis and the accelerometer measuring system will be described. This is followed by a discussion of the μg-data with respect to their potential origins.

Origins of Main Disturbances

It is one of the unique possibilities of space flight that a freely orbiting spacecraft offers a virtually zero-gravity state to its interior objects without time limitations by trajectory kinematics. For the spacecraft center of mass (CM), the gravitational force is balanced by the centrifugal force. Zero gravity, however, is an ideal state that cannot be accomplished completely in a real spacecraft due to a number of deviations from the model of a freely drifting mass point that result in small gravity-like disturbances. The origins of those disturbances, being of primary importance to the analysis of the μg-data presented, may be grouped with respect to their nature as follows.

Due to *external* forces, mainly the residual atmospheric drag, the orbiter is not in a freely drifting state, giving rise to a quasi steady acceleration a_d of the CM, acting in opposite direction to the orbital velocity vector. The level of a_d vs altitude as predicted for various orbiter flight modes is depicted in Fig. 1. For the SL-1 nominal flight altitude of 250 km, a maximum of $a_d = 5.10^{-6}\ g_o$ was to be expected for the attitude with the largest projected cross-sectional area.

Received Sept. 26, 1985; presented as Paper 85-7026 at the AIAA Shuttle Environment and Operations II Conference, Houston, TX, Nov. 13-15, 1985; revision received June 26, 1986.

*Mechanical Engineer, Institute for Space Simulation.
†Payload Specialist.

Additional transient external forces may result from operational activities such as thruster firings for attitude control or water dumps. These forces in general also exert a torque to the vehicle, resulting in transient rotational acceleration during the thruster firing event followed by a quasisteady acceleration period due to a constant rotation around the CM.

The mass allocation inside a spacecraft is, in general, changing due to the motion of mechanical parts, crew activities, etc., resulting in *internal* forces. These forces do not involve a momentum change to the spacecraft CM system. Impulses caused by internal forces are always compensated by equal and opposite impulses with a time delay, resulting in an excitation of the flexibility modes of the spacecraft. The induced transient acceleration, called *g*-jitter, is characterized by a broad frequency spectrum. Even though *g*-jitter may reach high peak values, the resulting displacements of particles with respect to the CM are small because of its compensated and random nature.[2]

A spacecraft is an *extended* body. For objects located off the CM, gravity and centrifugal forces are not balanced completely, giving rise to a "tidal acceleration" a_t that is proportional to the displacement r from CM. Its largest gradient is along the vector R

$$a_{t,z} = k \cdot r_z \tag{1}$$

where $k = 4.2 \cdot 10^{-7}$ g/m in case of the Gravity Gradient Mode and $h = 250$ km altitude.[3]

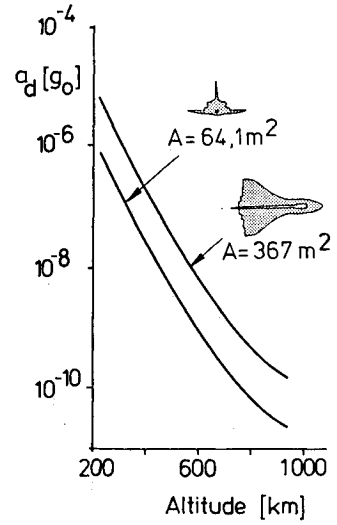

Fig. 1 Calculated effects of atmospheric drag on the Orbiter ($m = 90\,718$ kg).[4]

Table 1 Coordinates of the CM and μg-sensor in the Orbiter Structural Coordinate System (Fig. 2)[4]

Center of mass		
$r_{o,CM}$	$x_{o,CM} = 27.139$ m	
	$y_{o,CM} = -0.005$ m	
	$z_{o,CM} = 9.585$ m	
μg-sensor		
$r_{o,s}$	$x_{o,s} = 26.621$ m	
	$y_{o,s} = 1.249$ m	
	$z_{o,s} = 11.188$ m	
Displacement of μg-sensor from CM		
$d = r_{o,s} - r_{o,CM}$	$x_d = 0.518$ m	
	$y_d = 1.254$ m	
	$z_d = 1.603$ m	
	$d = 2.100$ m	

Payload and Accelerometer

The STS/SL-1 system, flown in a circular orbit of 250 km altitude, had a total on-orbit mass of $m = 89{,}6 \cdot 10^3$ kg. The locations of the CM and the *g*-sensor are listed in Table 1 for the coordinate system defined in Fig. 2.[4,5] The internal payload configuration of SL-1 and the position of the MSDR within Spacelab are shown in Fig. 3.[6] The MSDR consisted of

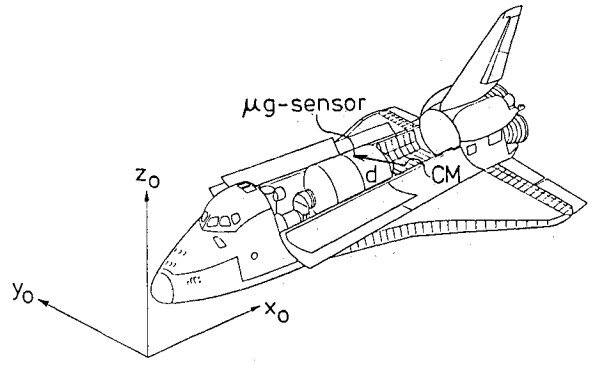

Fig. 2 Orbiter Structural Coordinate System, center of mass (CM) and μg-sensor.

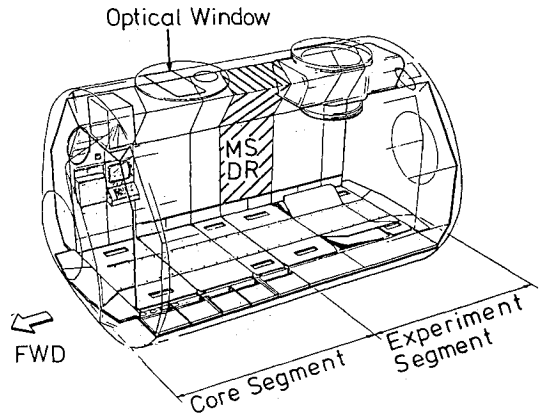

Fig. 3 Spacelab interior and location of the Material Science Double Rack (MSDR).

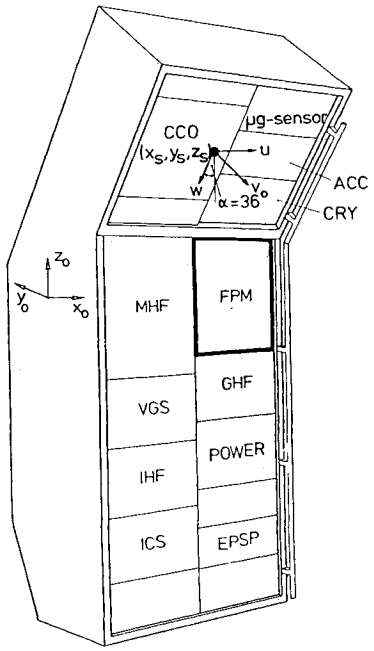

Fig. 4 MSDR and coordinate system of the μg-sensor. (For abbreviation see Table 2.)

several experiment facilities, support systems for cooling, power, vacuum and gas provisions, and a Central Console for monitoring, recording, and control functions (Table 2 and Fig. 4).

The g-sensor used was a three-axis accelerometer (QA-1200 Q-Flex, Sundstrand Data Control) consisting of three single-axis sensors oriented in coordinates u, v, w as indicated in Fig. 4. The operating principle of each sensor is based on the movement of a proof mass due to acceleration in a magnetic field. In a servo amplifier, a current is induced proportional to the acceleration and rebalances the proof mass to its neutral position.

The sensor has a resolution of $10^{-6}\ g_o$, a temperature coefficient of $10^{-5}\ g_o/°C$, and a frequency response of $\pm 10\%$ for 800 Hz. The accelerometer system had been calibrated prior to the final mounting into the MSDR. The measurement range was between 10^{-5} and $10^{-2}\ g_o$ for all six ($+u$, $+v$, $+w$, $-u$, $-v$, $-w$) directions. Peak values of the acceleration within time intervals of $\Delta t = 1$ s were detected for the six directions.

Data Analysis

The accelerometer was operated in a peak detection mode to reduce the total amount of data. From an analog random response of the sensor depicted in Fig. 5, the peak values indicated by the two-step functions $\bar{a}$ would be detected in the positive and negative direction of the coordinate considered. The lowest detectable limit $\bar{a}_{\min}$ is determined either by constant contributions to the μg-level, e.g., by the atmospheric drag, or by those harmonics with frequencies $f > 1$ Hz being exited by rotating machines, transport mechanisms, etc.

Both types in general cannot be distinguished from an $\bar{a}$ plot. Therefore, measurement results obtained by peak detection are primarily suited to analyze transient accelerations.

In the following section, examples of different classes of disturbances will be discussed with respect to their origins as identified by correlation with the SL-1 Post Mission Composite Timeline and the As-flown Attitude Timeline. The examples are subdivided into vehicle- and experiment-induced perturbations, the latter also including those originating from crew activities.

Vehicle Induced Disturbances

Atmospheric Drag

As previously discussed, the maximum drag acceleration is of the order of $a_d = 5 \cdot 10^{-6}\ g_o$ (Fig. 1). This is overwhelmed by $\bar{a}_{\min}$ throughout the measuring time. Hence, the variations of a_d due to attitude changes cannot be observed in the data.

"Tidal" Acceleration

Due to the displacement of the μg-sensor from the CM by $d = 2.1$ m (Table 1 and Fig. 2), the maximum tidal acceleration

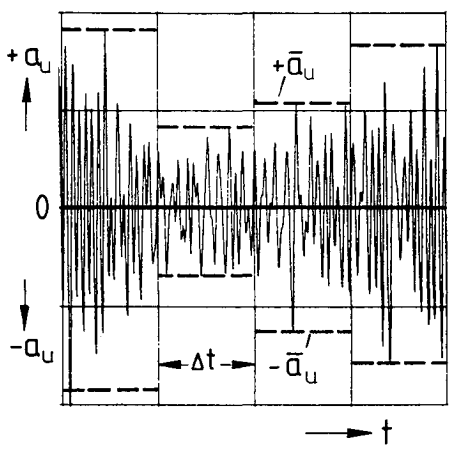

Fig. 5 Principle of the peak detection method.

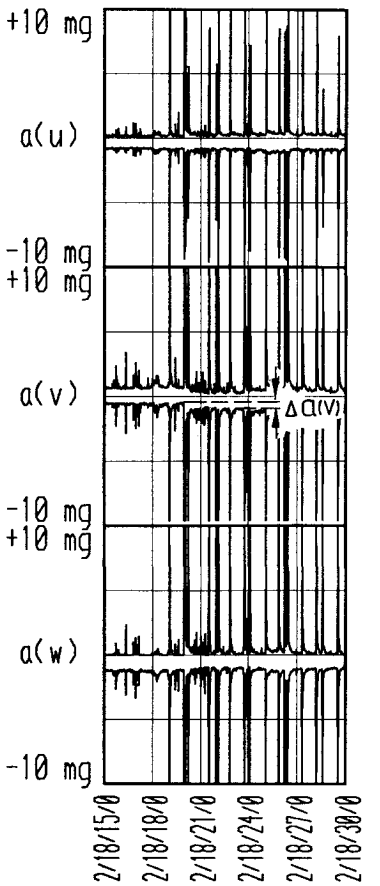

Fig. 6 Effects of Orbiter rotation around the x axis.

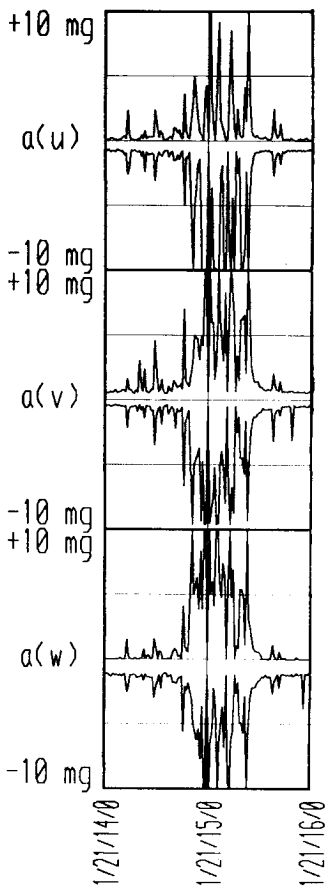

Fig. 7 Orbit trim burn 2; abscissa: mission elapsed time, day/hrs/min/s.

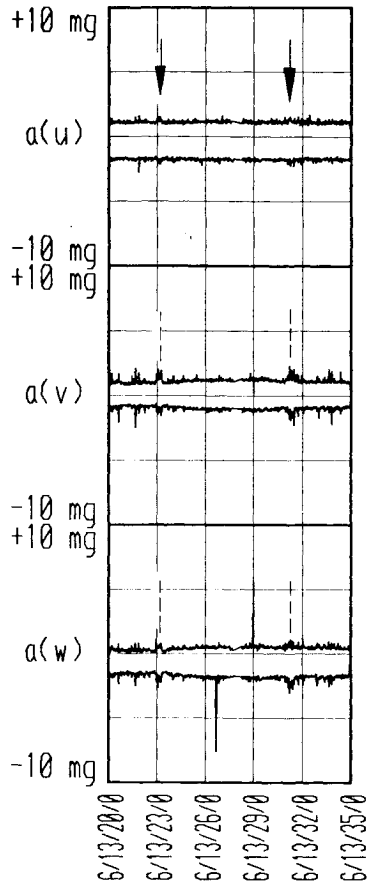

Fig. 8 Effects of two RCS thruster firings.

is, according to Eq. (1), $a_{t,z} = 9 \cdot 10^{-7} g_o$ and thus below the resolution of the sensor.

Vehicle Rotation

The maximum roll rate occurring during the measuring time of SL-1 was

$$\omega_x = 2.4 \text{ deg/s } (\omega_y = \omega_z = 0)$$

resulting in a centrifugal acceleration at the location of the μg-sensor of

$$a_c = 3.6 \cdot 10^{-4} g_o$$

Projection of ac on the v, w coordinates yields

$$a_{c,v} = -3.5 \cdot 10^{-4} g_o$$

$$a_{c,w} = -1.0 \cdot 10^{-4} g_o$$

The contribution of rotation to the total acceleration field can be observed as a change of the baseline levels of $\bar{a}_{\min}$ in the v coordinate. This change is of the order of the calculated value, as indicated in Fig. 6.

Thruster Firings

Examples of the two types of thruster firings, namely 1) trim burn for orbital maintenance by means of the Orbiter Maneuvering System (OMS) as well as 2) thruster firing for attitude control by means of the Reaction Control System (RCS) will be discussed. Orbital maintenance has been performed once during the measuring time in SL-1 at the end of the second day. Figure 7 shows the μg-data plot during this event. Full scale ($10^{-2} g_o$) has been exceeded in all directions with the largest effect in $-x$ direction, in which the momenta were acting. Thruster firing of the RCS has a much smaller impact on the μg-level as may be seen from Fig. 8, a representative example of this kind of disturbance.

Table 2 Experiment facilities and support equipment of the MSDR

Experiment facilities
Isothermal heating facility (IHF)
Mirror heating facility (MHF)
Gradient heating facility (GHF)
Cryostat (CRY)
Fluid physics module (FPM)
Ultrahigh vacuum chamber
High-temperature thermostat (HTT)
Support equipment
Instrument cooling system (ICS)
Vacuum gas system (VGS)
Central console (CCO)

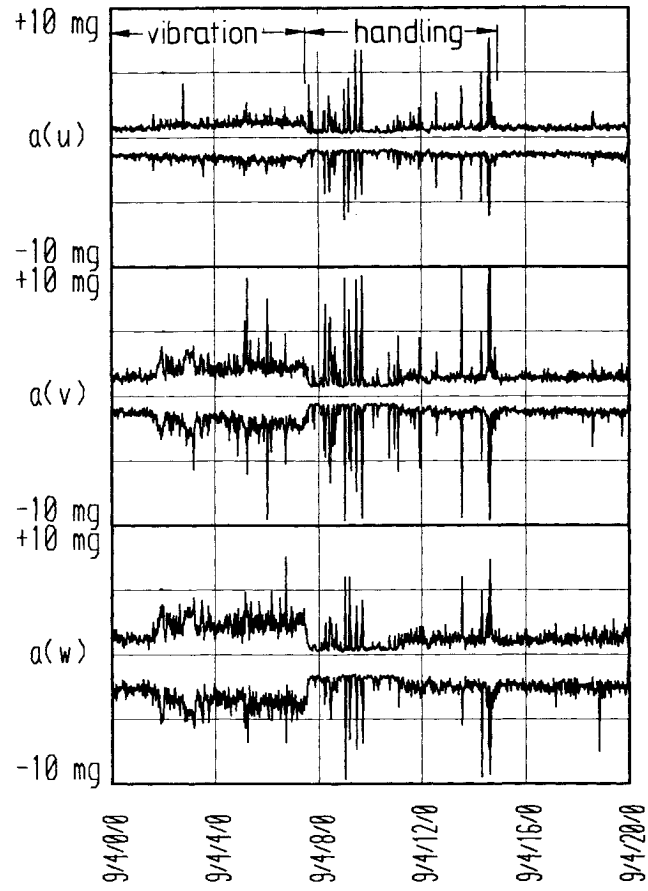

Fig. 9 Operation of the Fluid Physics Module (FPM), Experiment 1 ES 326.

MSDR-Induced Disturbances

The experiment facilities and auxiliary equipment installed in the MSDR naturally have a strong impact on the μg-level detected. Two examples are selected to demonstrate the consequences of both the design concept and the operation of a facility on the μg-environment: the Fluid Physics Module (FPM) and the Instrument Cooling System (ICS, Fig. 4).

Fluid Physics Module

The FPM caused g-jitter by rotating and vibrating parts and by procedures necessary to handle the samples, film changes, etc. For all handling activities, the FPM had to be extracted from the rack on telescopic slides.

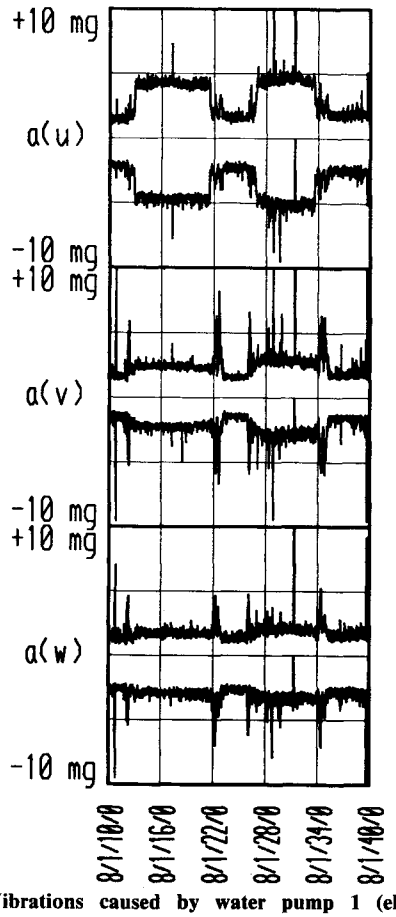

Fig. 10 Vibrations caused by water pump 1 (elevated level), switch-over to pump 2 (lower level).

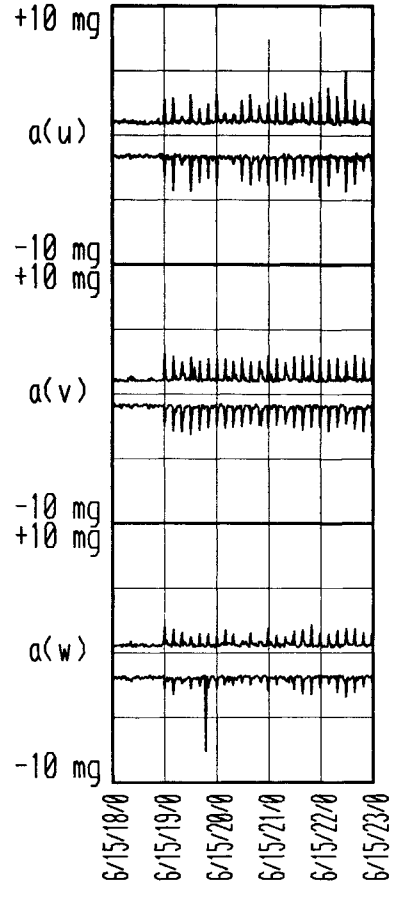

Fig. 11 Vibrations induced by film transport of the Metric Camera.

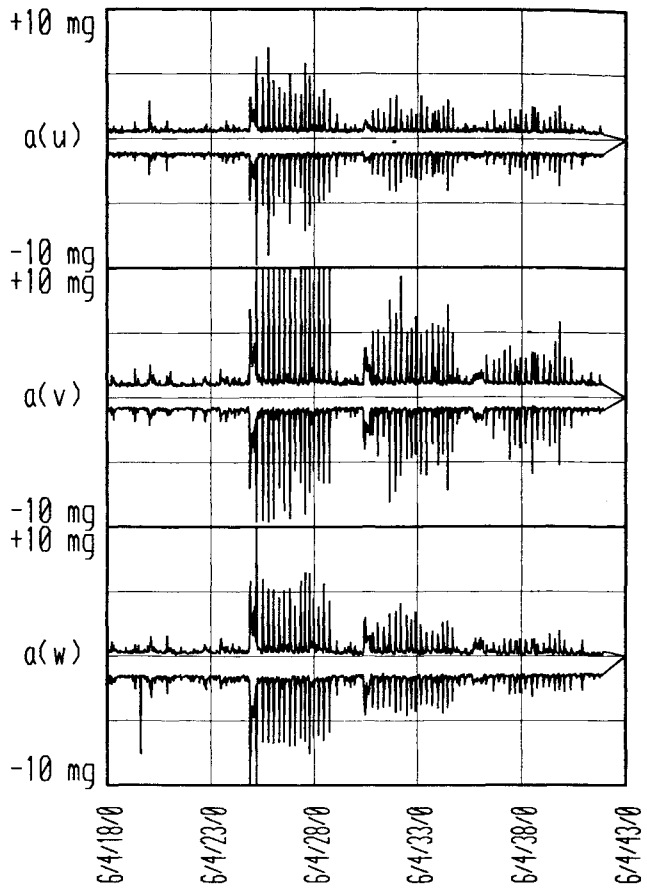

Fig. 12 Vibration pattern caused by Experiment 1 NS 102-F05 ("hop and drop").

Figure 9 shows a sequence of FPM-induced perturbations as measured during the performance of Experiment 1 ES 326. During the first phase, the facility was operated in its oscillation mode, causing relatively uniform vibration patterns. This phase was interrupted by a series of spikes with magnitudes up to full scale, originating from FPM extraction, film change and sample handling. This was followed by a quiet period.

As another example, vibrations originating from the water pumps of the Instrument Cooling System (ICS, Fig. 4) may be recognized from Fig. 10. Due to a failure of pump 1, causing noise and vibrations, the ICS had to be switched over to the pump 2. For that reason, pump 1 had been switched off several times, resulting in steps in the μg-level.

Other Experiments

The Metric Camera (Experiment 1 Ez 033) was installed at the Optical Window of the Spacelab Core Segment (Fig. 3). Regular spike patterns were generated in all directions as a result of the film transport with a frequency of 0.1 Hz (Fig. 11). The strongest effect was dominant along the u coordinate, in which the film transport occurred.

Another experiment strongly affecting the μg-level was of the Vestibular Experiment 1 NS 102-F05 "Hop and Drop." In this experiment, a Payload Specialist was accelerated along the z coordinate while "hopping" and then pulled down to the Spacelab floor by elastic cords. This exercise has been repeated several times in sequences with different pulling forces. Figure 12 shows the level of disturbances for three series performed with pulling forces of a relative magnitude of 1:2/3:1/3. The largest component is along the v coordinate, being the closest to the force vector.

Conclusions

In the light of these results, some first conclusions may be drawn concerning the design and operation of the Spacelab ex-

periment facilities and subsystems. As follows from the few examples discussed, the g-jitter levels are, with the exception of the Orbiter Trim Burn, determined by disturbances originating from the payload itself. The results of the analysis performed for the whole mission confirm this statement, even though not all patterns could be explained or correlated to a timeline event. This conclusion becomes obvious expecially from the FPM operations and the "Hop and Drop" experiment.

Various precautions are possible and necessary to reduce the μg-levels. Concerning some experiment facilities, e.g., the FPM, the design concept has to be improved drastically by minimizing the number of moving parts during operation and handling, taking damping precautions, decoupling disturbing units (e.g., motors, fans) from experiment facilities, etc. Another fact, the need for dedicated missions, has been discussed frequently in the past. The D1-Mission, for instance, is a step in this direction. In contrast to that, SL-1 had the character of a demonstration mission rather than of a μg-dedicated payload.

In addition to the design and operational precautions for the payload, the μg-measuring technique aboard Spacelab has to be improved. The peak detection method applied to SL-1 allows the analysis of the transient contributions to the g-jitter and the correlations to their origins. However, steady-state contributions are hard to identify. This method also suffers from the disadvantage that, for the same reason, any measurement offset of the system cannot be determined and eliminated from the μg-data. For sufficient support to the experimenters, the steady-state level as well as the frequency spectrum at the location of critical experiments has to be supplied.

Acknowledgment

The authors are indebted to Dr. N. Trappen (DFVLR) for his valuable support in processing the μg-flight data and to Mr. R. Jilg (DFVLR) for his assistance with the analysis of the data.

References

[1]"Results of Spacelab-1," *5th European Symposium on Material Sciences Under Microgravity*, DFVLR/ESA, ESA Sp-222, Schloß Elmau, FRG, Nov. 1984.

[2]Naumann, R.J., "Susceptibility of Material Processing Experiments to Low Level Acceleration," *Proceedings of Spacecraft Dynamics as Related to Laboratory Experiments in Space*, NASA Marshall Space Flight Center, May 1979, NASA CP-2199, 1981, pp. 63-68.

[3]Bauer, H.F., "Environmental Effects on Microgravity Experiments," *Zeitschrift für Flugwissenschaften*, Vol. 6, 1982, pp. 184-194.

[4]*Spacelab Payload Accomodation Handbook*, NASA/ESA, 1982.

[5]*Space Shuttle STS-9*, NASA, Vol. 2, MSFC-RTT-1038, 1984.

[6]"Spacelab Mission 1 Experiment Descriptions," NASA/TM-78173, ESA/FSLP-EX-001, 1978, p. 1.